Identification of critical stacking faults in thin-film CdTe solar cells

Su-Hyun Yoo, Keith T. Butler, Aloysius Soon, Ali Abbas, John M. Walls, and Aron Walsh

---

Articles you may be interested in

Modeling of the effects of charge transport on voltage-dependent photocurrent in ultrathin CdTe solar cells
J. Vac. Sci. Technol. A 31, 061201 (2013); 10.1116/1.4813323

Discussion of some "trap signatures" observed by admittance spectroscopy in CdTe thin-film solar cells
J. Appl. Phys. 108, 064501 (2010); 10.1063/1.3475373

Nonlinear shunt paths in thin-film CdTe solar cells
J. Appl. Phys. 97, 054503 (2005); 10.1063/1.1856216

Lock-in thermography and nonuniformity modeling of thin-film CdTe solar cells
Appl. Phys. Lett. 84, 729 (2004); 10.1063/1.1645322

Deep-level impurities in CdTe/CdS thin-film solar cells
J. Appl. Phys. 88, 7175 (2000); 10.1063/1.1326465

Identification of critical stacking faults in thin-film CdTe solar cells

Su-Hyun Yoo,[1,2] Keith T. Butler,[2] Aloysius Soon,[1] Ali Abbas,[3] John M. Walls,[3,a)] and Aron Walsh[1,2,b)]

[1]Global E3 Institute, Department of Materials Science and Engineering, Yonsei University, Seoul 120-749, South Korea
[2]Centre for Sustainable Chemical Technologies and Department of Chemistry, University of Bath, Bath BA2 7AY, United Kingdom
[3]Centre for Renewable Energy Systems Technology, School of Electronic, Electrical and Systems Engineering, Loughborough University, Leicestershire LE11 3TU, United Kingdom

Cadmium telluride (CdTe) is a p-type semiconductor used in thin-film solar cells. To achieve high light-to-electricity conversion, annealing in the presence of $CdCl_2$ is essential, but the underlying mechanism is still under debate. Recent evidence suggests that a reduction in the high density of stacking faults in the CdTe grains is a key process that occurs during the chemical treatment. A range of stacking faults, including intrinsic, extrinsic, and twin boundary, are computationally investigated to identify the extended defects that limit performance. The low-energy faults are found to be electrically benign, while a number of higher energy faults, consistent with atomic-resolution micrographs, are predicted to be hole traps with fluctuations in the local electrostatic potential. It is expected that stacking faults will also be important for other thin-film photovoltaic technologies. © 2014 AIP Publishing LLC. [http://dx.doi.org/10.1063/1.4892844]

Cadmium telluride (CdTe) is a II-VI semiconducting material used in thin-film photovoltaic (PV) devices. It exhibits intrinsic p-type conductivity with a direct optical band gap close to 1.5 eV, as well as a high optical absorption coefficient of $5 \times 10^5 \, cm^{-1}$.[1] Recently, CdTe/CdS devices with light-to-electricity conversion efficiencies in excess of 20% for small area cells and 16% for modules have been reported.[2]

It is well documented that an annealing treatment in the presence of $CdCl_2$ is essential for enhancing the photovoltaic performance of CdTe. However, the mechanisms causing this improvement are still under debate, with arguments based on changes in point defect concentrations, passivation of recombination centers at grain boundaries, and changes in the film morphology.[3,4] The most recent model, presented by Li et al.,[5] emphasised the substitution of Cl atoms for Te atoms at grain boundaries, which form n-type regions that facilitate electron-hole separation.

Recently, experimental evidence has shown that a high density of stacking faults is present in the as-deposited films of CdTe.[6] Also, it is now established that the stacking faults are removed by the cadmium chloride annealing treatment, and the cell efficiency is dramatically enhanced. The current-voltage curve in Figure 1 shows the radical change in performance caused by the chemical treatment. Prior to treatment, the device behaves essentially as a resistor; after the treatment, 12% conversion efficiency is achieved.

The application of first-principles techniques to investigate stacking faults in crystalline materials is well developed,[7] and stacking faults in tetrahedral semiconductors have been the subject of many investigations.[8–11] Nonetheless, there is currently little understanding of the connection between these faults and photovoltaic performance in CdTe devices.

In this work, we report a joint experimental and computational investigation into the role of stacking faults in CdTe with regards to the thermodynamics and electronic structure. We construct model geometries compatible with high-resolution transmission electron microscopy (HRTEM) data and investigate the formation of extended defects via Kohn-Sham density-functional theory (DFT). The faults considered in this work include intrinsic and extrinsic stacking faults with two kinds of coordination, as well as twin boundaries. The principal finding is that a subset of stacking faults introduce hole traps into the material that will inhibit photo-generated carrier collection, while the majority of low-energy faults are benign and should not affect device performance. The faults are confirmed experimentally to be removed by annealing in the presence of $CdCl_2$, explaining one of the roles of this treatment in the production of
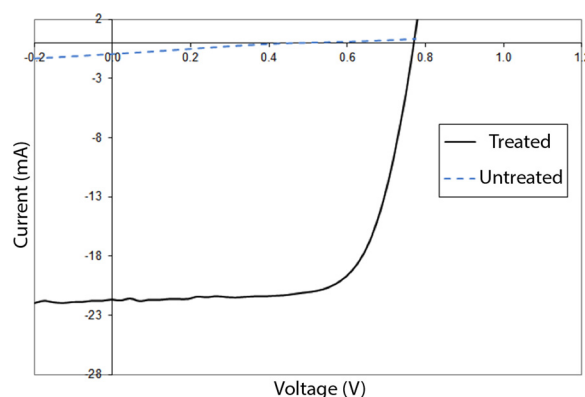

FIG. 1. Current-voltage characteristics of an untreated thin-film CdTe photovoltaic cell ($1 \, cm^2$) compared with a cadmium chloride treated device.

a)E-mail: j.m.wall@loughborough.ac.uk
b)a.walsh@bath.ac.uk

high-quality PV material. These findings are important for the design of optimal production routes of CdTe solar cells. Furthermore, the availability of high-quality crystals of CdTe makes it an excellent prototype for studying the formation and properties of lattice defects, as many other tetrahedral semiconductors are promising PV absorber materials (e.g., kesterite structured Cu_2ZnSnS_4).

Solar Cell Fabrication—Thin-film CdTe solar cells were deposited using close space sublimation (CSS) in an all-in-one vacuum process. The devices were deposited on NSG-Pilkington TEC10 fluorine-doped tin oxide coated on 3 mm soda lime glass in a superstrate configuration. The glass superstrate was passed though different chambers at 40 mTorr vacuum, held a few millimetres above graphite boats. The boats were heated to 650 °C with the different materials, which then sublimed onto the superstrate surface. An n-type cadmium sulphide was deposited followed by an approximately 3 μm thick layer of CdTe. One of the samples remained untreated, while the second sample was exposed to the activation treatment. The cadmium chloride was sublimated to a thickness of ∼3 μm, and then the sample was heated for 8 min at 400 °C in a 2% oxygen atmosphere, causing the $CdCl_2$ layer to evaporate. This was followed by a copper doping process by sublimating CuCl onto the CdTe surface. These two circular small area devices of 1 cm^2 area were then finished by applying a graphite-paste back electrode.

High-resolution Microscopy—Analysis using HR-TEM was carried out using an FEI Tecnai F20 TEM. The grain was tilted to the ⟨011⟩ zone axis to observe along the [111] plane to enable imaging of the lattice. TEM samples were prepared by focused ion beam (FIB) milling using a dual beam FEI Nova 600 Nanolab. A standard *in situ* lift out method was used to prepare cross-sectional samples through the coating into the glass substrate. A platinum over-layer was deposited to define the surface and homogenize the final thinning of the samples. Finally, a low voltage ion clean-up was used on each side of the sample. The energy of the ion beam was reduced to 5 keV using a beam current of 70 pA. The sample was tilted 2° extra each side of 52° (in-line with the ion beam) and brushed with the ion beam for 2 min. This procedure reduces the amount of ion implantation and damage and results in improved lattice imaging.

Materials Modelling—All electronic structure calculations are performed in the VASP code[12,13] based on the projector augmented wave (PAW) approach.[14] The plane-wave basis set is implemented with energy cut-off of 300 eV, and a gamma-centered *k*-point grid of $6 \times 6 \times 6$ is used for the reciprocal space sampling of zinc-blende (ZB) structured CdTe ($6 \times 6 \times 1$ for the (111) oriented supercells). Structural optimization was carried out until all atomic forces are less than 0.01 eV Å^{-1}. For the exchange-correlation functional, the generalized gradient approximation (GGA) due to Perdew *et al.*, known as PBEsol,[15] is employed for structure optimization. The HSE06 hybrid functional[16,17] is used for a more accurate description of the electronic structure[18–20] with single-point calculations on pre-optimised structures. The calculated lattice constant and band gap energy of ZB CdTe, 6.496 Å (from PBEsol) and 1.49 eV (from HSE06), show very good agreement with the experimental and theoretical data, 6.482 Å and 1.50 eV.[1,21,22] From the equilibrium

bulk structure, (111) oriented supercells containing stacking faults (SF)—11 atomic layers (AL) for intrinsic SF and 13 AL for other SF systems—have been generated by lattice transformations in the code VESTA.

The stacking-fault energy (SFE), conventionally reported in units of mJ/m^2, is defined here as the total energy difference between structures which contain SF and the perfect bulk crystal.[23] Specifically, the SFE is calculated from

$$SFE = \frac{1}{2A}\left(E^{\text{total}}_{\text{SF supercell}} - nE^{\text{total}}_{\text{ZB bulk}}\right),$$

where A is the area of the stacking fault, $E^{total}_{SF\,supercell}$ is the total energy of the defective supercell with n formular units, and $E^{total}_{ZB\,bulk}$ is the total energy of bulk CdTe.

Representative HRTEM images from the cross-section of a CdTe thin-film before and after annealing treatment are shown in Figure 2. The micrographs illustrate the decrease of SF density due to annealing treatment. Simultaneously, twin boundaries appear in the treated sample (or their presence is simply highlighted by the removal of the stacking faults).

In order to investigate the role of stacking faults, we model the supercell structures with a range of SFs. We considered stacking faults of the following types: intrinsic (ABCACABC), extrinsic (ABCABACABC), double intrinsic (ABCACACABC), and the formation of a twin boundary (ABCABACBA). Within the categories of intrinsic and extrinsic stacking faults, two further categorizations are possible, based on the local coordination environment of Te at the stacking fault. The first is octahedral with six Cd neighbours, shown in Figure 3(a). The second is tetrahedral with respect to Cd coordination as shown in Figure 3(b). All structures were analysed in terms of formation enthalpy, geometric structure, and electronic structure.

The calculated heat of formation for each SF is shown in Table I. The tetrahedral stacking faults have significantly lower formation energies, ranging from 26.7 to 36.7 mJ/m^2, than those of the polytype structures. These values are in good agreement with those found in other tetrahedral semiconductors. The SFEs of both intrinsic and extrinsic SF systems with polytype coordination are 219.5 and 234.6 mJ/m^2, respectively. Based on the calculated stacking fault energies, under a regime of thermodynamic control, one would expect a statistical distribution of tetrahedral and polytype SFs, with an abundance of the former. The twin boundary structures, Figure 3(c), display
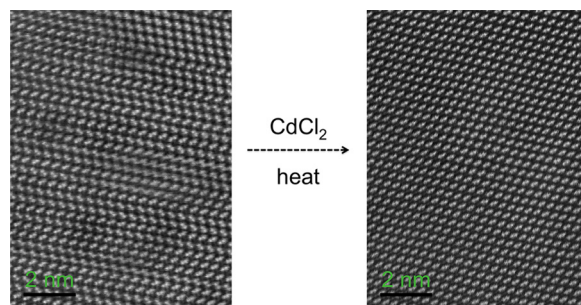

FIG. 2. High-resolution TEM image of CdTe before (left) and after (right) annealing treatment. An atomistic model for the stacking faults observed is given in Figure 3.
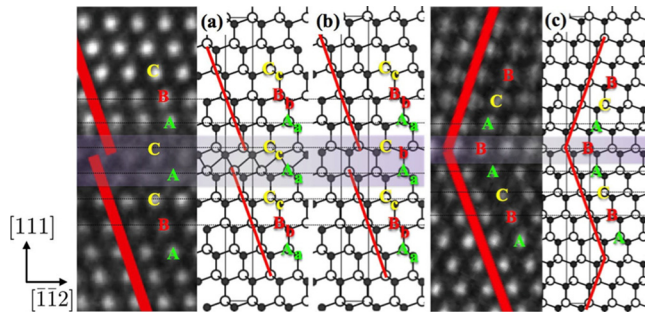
FIG. 3. Structural analysis of HRTEM images (from Figure 2) and atomistic modelling for (a) polytype and (b) tetrahedral intrinsic stacking faults (11 atomic layers) and (c) twin boundary (13 atomic layers). The white and black atoms refer to Cd and Te, respectively. The purple shaded region indicates the stacking fault location; the horizontal dotted lines represent the matching of the Cd atomic layers in the model and HRTEM structures. Upper- and lower-case letters represent Cd and Te, respectively, where the perfect fcc crystal follows AaBbCc.

the smallest SFE of only 16.2 mJ/m^2, which is consistent with their apparent resistance to annealing.

In order to assess which stacking faults are present in the as-grown films of CdTe, we have performed a direct comparison of the stacking sequences observable in HRTEM with the geometry optimised model stacking sequences. This structural analysis reveals an excellent agreement between the DFT calculated structure of the intrinsic SF geometry and the micrograph, Figures 3(a) and 3(b). A systematic search of HRTEM over larger areas did not reveal any structures with the characteristics of an extrinsic stacking fault; therefore, we conclude that such structures are not present in any significant concentration. We have also developed an atomistic model for the twin boundary, which shows very good agreement with the feature that emerges in the treated sample in Figure 3(c).

Having established the geometric structure of the experimentally observed stacking faults, we can analyse the changes in electronic structure to assess their effect on PV performance. The electrostatic (Hartree) potential in the plane of the defect is calculated as

$$\bar{v}(z) = \frac{1}{2} \int_A v(x, y, z) dx dy,$$

TABLE I. Calculated SFE and band gap for defective CdTe. Also listed is the aligned eigenvalue difference of VBM and conduction band maximum (CBM) compared to that of pure CdTe. The SFE is calculated using PBEsol, and all other properties using the hybrid HSE06 functional.

SF type		SFE (mJ/m^2)	E_g (eV)	ΔVBM (eV)	ΔCBM (eV)
Intrinsic					
	Tetrahedral	26.7	1.50	−0.02	0.00
	Polytype	219.5	1.38	0.11	0.00
Extrinsic					
	Tetrahedral	32.1	1.49	−0.01	−0.01
	Polytype	234.6	1.30	0.16	−0.03
Twin		16.2	1.48	−0.03	−0.04
Intrinsic×2					
	Tetrahedral	36.7	1.49	−0.01	−0.01

where A is the area of the unit cell in the plane. Since variations in the electrostatic potential can be obscured by the periodic fluctuations of potential with the lattice, we have also calculated a macroscopic average of the potential that smears out lattice-related oscillations

$$\bar{\bar{v}}(z) = \frac{1}{a} \int_{z-\frac{1}{2}}^{z+\frac{1}{2}} \bar{v}(z') dz',$$

where a is the length of the shortest periodically repeating unit of the structure in the direction perpendicular to the SF plane. Both potentials are plotted in Figure 4.

Analysis of the electrostatic potential reveals a fluctuation of 0.89 V in the macroscopic average of the potential for the polytype SF in the vicinity of the defect. Conversely, the tetrahedral SF shows no appreciable effect (see Figure 4).

The valence and conduction bands of CdTe are formed as a result of periodic potential including the Cd and Te atomic positions; defects that alter the periodicity can introduce hole
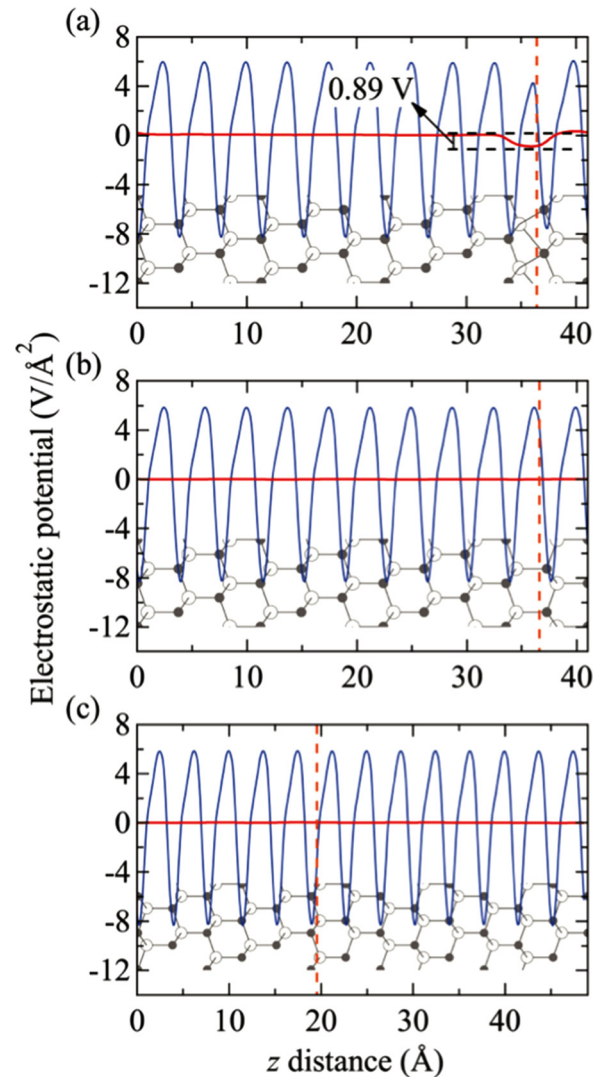

FIG. 4. Calculated electrostatic potential of intrinsic stacking faults with (a) polytype, (b) tetrahedral, and (c) twin boundary systems. The blue solid, red solid, and orange dotted lines represent the planar averaged electrostatic potential, macroscopic averaged electrostatic potential, and location of SF, respectively. Simultaneously, the supercells of each SF system are shown in below of graph with Cd (white empty ball) and Te (black solid ball).

or electron trap states due to a spatial inhomogeneity in the electrostatic potential. Examples of this behavior in solar cell materials are disorder of Cu and Zn atoms in Cu_2ZnSnS_4 and alignment of molecular dipoles on $CH_3NH_3PbI_3$.[24,25] The perturbation of the electrostatic potential fluctuation, caused by the stacking faults, on the band structure of CdTe is presented in Table I. The valence band maximum (VBM), composed primarily of Te 5p orbitals, is destabilised by the positive potential change. The perturbation, following dielectric screening, amounts to a VBM shift of 0.16 eV, and a relative decrease of 0.11 eV in the band gap.

The calculations suggest that these stacking faults will be a source of non-radiative recombination. The valence band energy is destabilized in the region of the defect (lower ionization potential), such that they will attract hole carriers. Trap states are introduced into the band gap (at VBM + 0.16 eV) that will capture free holes in the material, resulting in an increased probability of electron-hole recombination and lower cell voltages. The effect may be particularly strong owing to the two dimensional nature of the defects (and the associated fluctuations in potential), in contrast to the localized perturbation caused by an isolated point defect. The recombination kinetics should be similar to those found for interface and grain boundary effects, where the trap density and recombination flux per unit area are the critical descriptors.

In contrast to the polytype SF, the twin boundary considered here shows an electrically benign behavior. The electrostatic potential, shown in Figure 3(c), causes no significant perturbation in the region of the boundary. The changes in both the VBM and band gap are negligible, within the accuracy of the computational method. While twin boundaries are frequently observed in thin-film samples,[26,27] the type considered here should not have any appreciable impact on photovoltaic device performance for CdTe.

In conclusion, we have studied the origin of the performance increase in CdTe solar cells annealed in the presence of $CdCl_2$. A combination of experimental measurements and computations suggests a coherent picture, whereby extended stacking fault defects—acting as source of hole traps—limit the performance. Experimentally, the removal of high density of SFs and the appearance of twin boundaries are observed in HRTEM micrographs of CdTe thin-films before and after annealing treatment. From a computational screening, we find that the intrinsic polytype SF results in a significant fluctuation of the electrostatic potential (0.89 V) and an upward shift of the valence band in the region of the SF. Moreover, we confirm that twin boundaries are electrically benign and should not affect the photovoltaic performance. This correlates with the observation that twin boundaries are always observed in the cadmium chloride treated material and that this material generates high-conversion efficiency devices. The microscopic role of $CdCl_2$ (and the recently reported $MgCl_2$[28] in this process is not yet clear, e.g., the effect of mass transport on the rate of polytype conversion, and will be the subject of further investigations. This study highlights the potentially critical role of stacking fault defects and has implications for the treatment and production of CdTe, and indeed tetrahedral semiconductors in general, for solar cell applications.

[1]A. Luque and S. Hegedus, *Handbook of Photovoltaic Science and Engineering*, 2nd ed. (John Wiley & Sons, Ltd, West Sussex, 2011).

[2]M. A. Green, K. Emery, Y. Hishikawa, W. Warta, and E. D. Dunlop, Prog. Photovolt: Res. Appl. **22**, 1 (2014). Note that First Solar reported a certified cell efficiency of 20.4% in February 2014.

[3]M. A. Berding, Phys. Rev. B **60**, 8943 (1999).

[4]L. Zhang, J. L. F. Da Silva, J. Li, Y. Yan, T. A. Gessert, and S.-H. Wei, Phys. Rev. Lett. **101**, 155501 (2008).

[5]C. Li, Y. Wu, J. Poplawsky, T. J. Pennycook, N. Paudel, W. Yin, S. J. Haigh, M. P. Oxley, A. R. Lupini, M. Al-Jassim, S. J. Pennycook, and Y. Yan Phys. Rev. Lett. **112**, 156103 (2014).

[6]A. Abbas, G. D. West, J. W. Bowers, P. Isherwood, P. M. Kaminski, B. Maniscalco, P. Rowley, J. M. Walls, K. Barricklow, W. S. Sampath, and K. L. Barth IEEE J. Photovoltaics **3**, 1361 (2013).

[7]P. S. Branicio, J. Y. Zhang, and D. J. Srolovitz, Phys. Rev. B **88**, 064104 (2013); J. L. Yin, M. L. Hu, Z. Yu, C. X. Zhang, L. Z. Sun, and J. X. Zhong, Phys. B **406**, 2293 (2011).

[8]G. C. Hua, D. C. Grillo, T. B. Ng, C. C. Chu, J. Han, and R. L. Gunshor, J. Electron. Mater. **25**, 263 (1996).

[9]T. Walter and D. Gerthsen, Ultramicroscopy **81**, 279 (2000).

[10]T. Passow, H. Heinke, J. Falta, K. Leonardi, and D. Hommel, Appl. Phys. Lett. **77**, 3544 (2000).

[11]P. B. Dayal, B. R. Mehta, Y. Aparna, and S. M. Shivaprasad, Appl. Phys. Lett. **81**, 4254 (2002).

[12]G. Kresse and J. Hafner, Phys. Rev. B **47**, 558 (1993).

[13]G. Kresse and J. Furthmüller, Phys. Rev. B **54**, 11169 (1996).

[14]G. Kresse and D. Joubert, Phys. Rev. B **59**, 1758 (1999).

[15]J. P. Perdew, A. Ruzsinszky, G. I. Csonka, O. A. Vydrov, G. E. Scuseria, L. A. Constantin, X. Zhou, and K. Burke, Phys. Rev. Lett. **100**, 136406 (2008).

[16]J. Heyd, G. E. Scuseria, and M. Ernzerhof, J. Chem. Phys. **118**, 8207 (2003).

[17]J. Heyd, G. E. Scuseria, and M. Ernzerhof, J. Chem. Phys. **124**, 219906 (2006).

[18]S.-H. Yoo, A. Walsh, D. O. Scanlon, and A. Soon, RSC Adv. **4**, 3306 (2014).

[19]M. A. L. Marques, J. Vidal, M. J. T. Oliveira, L. Reining, and S. Botti, Phys. Rev. B **83**, 035119 (2011).

[20]W. Li, C. F. J. Walther, A. Kuc, and T. Heine, J. Chem. Theory Comput. **9**, 2950 (2013).

[21]O. Madelung, M. Schlz, and H. Weiss, *Landolt-Börnstein: Numerical Data and Functional Relationships in Science and Technology*, vol. 17 (Springer, Berlin, 1982).

[22]J.-H. Yang, S. Chen, W.-J. Yin, X. G. Gong, A. Walsh, and S.-H. Wei, Phys. Rev. B **79**, 245202 (2009).

[23]Q.-X. Dai, A.-D. Wang, X.-N. Cheng, and X.-M. Luo, Chin. Phys. **11**, 596 (2002).

[24]T. Gokmen, O. Gunawan, T. K. Todorov, and D. B. Mitzi, Appl. Phys. Lett. **103**, 103506 (2013).

[25]J. M Frost, K. T. Butler, and A. Walsh, APL Mater. **2**, 081506 (2014).

[26]K. Durose and G. J. Russell, J. Cryst. Growth **101**, 246 (1990).

[27]Y. Yan, M. M. Al-Jassim, and K. M. Jones, Thin Solid Films **389**, 75 (2001).

[28]J. D. Major, R. E. Treharne, L. J. Philips, and K. Durose, Nature **511**, 334 (2014).